NeuroImage 51(1), 274-279 (2010)

The change in cerebrovascular reactivity between 3T and 7T measured using graded hypercapnia

Ian Driver[1], Nicholas Blockley[1], Joseph Fisher[2], Susan Francis[1], Penny Gowland[1].

[1] Sir Peter Mansfield Magnetic Resonance Centre, School of Physics and Astronomy, University of Nottingham, Nottingham, UK

[2] Department of Anesthesia, University Health Network, University of Toronto, Toronto, Canada

doi: 10.1016/j.neuroimage.2009.12.113

Abstract

Mapping cerebrovascular reactivity (CVR) to hypercapnia is important both clinically and for improved understanding of the haemodynamic properties of the BOLD effect. In this work BOLD/R_2* CVR was investigated by using a device which provided small, repeatable and stable steps in $P_{ET}CO_2$, whilst maintaining a steady $P_{ET}O_2$ level. Significant CVR was observed in both grey and white matter at both 3 & 7T, whilst an approximately linear relationship found between R_2* CVR and field strength has implications for BOLD models and calibration. Grey matter R_2* CVR was 0.066±0.004 s^{-1} $mmHg^{-1}$ at 3T and 0.141±0.008 $s^{-1}mmHg^{-1}$ at 7T. White matter R_2* CVR was 0.021±0.003 $s^{-1}mmHg^{-1}$ at 3T and 0.040±0.007 $s^{-1}mmHg^{-1}$ at 7T.

Introduction

The ability of the body to modulate cerebral blood flow (CBF) is important both clinically and in understanding the haemodynamic response to neuronal activation. The cerebral vasculature has considerable vascular constrictor and dilator reserves. CBF is very sensitive to changes in arterial PCO_2 (P_aCO_2), increasing 4-6% per 1 mmHg increase in P_aCO_2 (Noth et al. 2006; Pollock et al. 2009). On the other hand previous studies suggest mild hypercapnia does not significantly alter $CMRO_2$ (Davis et al. 1998; Chen and Pike 2009). Therefore in response to hypercapnia the concentration of deoxyhemoglobin [dHb] in venous blood decreases dramatically causing a BOLD signal. Cerebrovascular reactivity (CVR) as measured by BOLD MRI is defined as the change in BOLD signal in response to a change in P_aCO_2 and provides a measure of the capacity of vessels to react to a stimulus. This technique has been applied to map the regional distribution of CVR in cerebrovascular disease such as stroke and carotid artery stenosis and occlusion (van der Zande et al. 2005; Mandell et al. 2008). The BOLD CVR is also of particular interest since it is used in calibrated BOLD: either the functional BOLD response to a task is divided by the BOLD response to mild hypercapnia on a voxel-by-voxel basis, or alternatively the functional BOLD response to a task is used to estimate $\delta CMRO_2$ based on the model of Davis et al.(Davis et al. 1998).

Many studies (Kastrup et al. 2001; Vesely et al. 2001; van der Zande et al. 2005; Wise et al. 2007; Prisman et al. 2008) have measured BOLD CVR by inducing a step change in P_aCO_2. Since direct measurement of P_aCO_2 is invasive, the exhaled 'end-tidal' PCO_2 ($P_{ET}CO_2$) of expired gases is sampled instead. Cohen (Cohen et al. 2004) used a single step change in $P_{ET}CO_2$ (5% CO_2 for 3 minutes) and showed that BOLD CVR increased with field strength (considering 1.5, 4 & 7T). Mandell (Mandell et al. 2008) found a close correlation between BOLD and CBF changes in response to a single step

change in $P_{ET}CO_2$ of 10 mmHg $P_{ET}CO_2$. Hoge (Hoge et al. 1999) (1.25, 2.5, 3.75 and 5% CO_2) and Stefanovic (Stefanovic et al. 2006) (5, 7.5 and 10% CO_2) measured both CBF and BOLD signal changes in response to multiple steps in $P_{ET}CO_2$ to estimate $CMRO_2$. Posse (Posse et al. 2001) modulated $P_{ET}CO_2$ from 20-70 mmHg, to probe T_2* CVR over a large range. With the exception of Hoge (Hoge et al. 1999), all the studies have used large steps in $P_{ET}CO_2$ (≥10mmHg), to provide good contrast-to-noise ratio (CNR) in the CVR measurement. However, such large steps prevent a thorough examination of the relationship between CVR and P_aCO_2.

MR studies of CVR have variously studied changes in the BOLD signal or T_2*. However it is the change in R_2* (determined by the change in blood volume and oxygenation (Yablonskiy and Haacke 1994)) that is the primary haemodynamic response to an increase in blood flow, rather than the BOLD effect, which also depends on the baseline R_2* and potentially blood inflow effects.

The aim of this study was to assess the dependence of R_2* CVR on P_aCO_2 over the normal physiological range and to investigate how the BOLD signal resulting from this controlled challenge varies with field strength, between 3T and 7T. As field strength increases, the intrinsic signal-to-noise-ratio (SNR) and the R_2* and hence BOLD signal increases and the contribution of blood to the total signal decreases (Yacoub et al. 2001; van der Zwaag et al. 2009). Therefore a cross-field study of the effect of CVR on the BOLD signal will provide some insight into the underlying mechanisms of the BOLD effect. We used a RespirAct™ system (Thornhill Research Inc., Toronto, Canada) to apply precise, small, well tolerated, iso-oxic step changes in $P_{ET}CO_2$ in a pseudo random order. The BOLD and $P_{ET}CO_2$ data was analysed on a point by point basis to include data generated during the $P_{ET}CO_2$ transitions and thus sample a wider range of $P_{ET}CO_2$ levels.

Methods

Five healthy males with a mean age of 25 years (range 23-29 years) took part in the study. Approval for the study was obtained from the University of Nottingham Medical School Ethics Committee and all subjects gave written informed consent.

Control of end-tidal gas

A feed-forward, low gas flow system (RespirAct™, Thornhill Research Inc., Toronto, Canada) and a sequential gas delivery (SGD) breathing circuit (Figure 1) (Banzett et al. 2000; Slessarev et al. 2007) were used to target $P_{ET}CO_2$ and $P_{ET}O_2$ independently (Slessarev et al. 2007). Source gases used by the system were O_2, air, and two gas blends of N_2, CO_2 and O_2, so that all source gases were of safe O_2 concentrations. The Respiract™ follows the approach of Slessarev et al. (Slessarev et al. 2007) to calculate the required flows of these source gases into the SGD breathing circuit to attain the targeted $P_{ET}CO_2$ and $P_{ET}O_2$.

The system comprises of an inspiratory and exhaled gas reservoir. During gas delivery, the subject was instructed to empty the inspiratory gas reservoir with every breath. Additional inspired gas, if required, was then drawn from the exhaled gas reservoir through a second valve that opens once the inspiratory reservoir is collapsed (as previously exhaled gas has already equilibrated with the blood, breathing in this gas has no effect on gas exchange). Gas exchange is therefore determined solely by inhaling the gas supplied, independent of ventilation. The gas exchange for CO_2 and O_2 are controlled independently using the same approach (Slessarev et al. 2007). An important aspect of this system is that it reduces regional gas gradients in the lung, thus the $P_{ET}CO_2$ provides as good a measure of P_aCO_2 as direct arterial blood analysis (Ito et al. 2008).

Protocol

The face mask of the breathing circuit was placed comfortably on the face of the subject and skin tape (Tegaderm, 3M Health Care, St.Paul, MN) was used to assure an air-tight seal to the face. The subject was then positioned in the magnet. The gas supply and sample tubing were passed through a wave guide to the control room where they were connected to the Respiract™. Prior to performing the CO_2 challenge, subjects simply breathed medical air through the system. Target end-tidal values were entered into the Respiract™, which prospectively calculated the delivered gas concentrations to achieve the targets based on estimated metabolic values. During the respiratory challenge, subjects were visually cued to breathe at approximately 15 breaths/min (between 6 and 24 breaths/min, the actual breathing frequency does not affect the results (Ito et al. 2008)) and sufficiently deep to always empty the inspiratory gas reservoir. Prior to placing the subject in the magnet, required metabolic values were estimated iteratively by targeting a baseline (40 mmHg $P_{ET}CO_2$, 100 mmHg $P_{ET}O_2$) and refining the metabolic estimates so that the baseline is achieved. The hypercapnic challenge consisted of an initial 3 minute of baseline $P_{ET}CO_2$ (40 mmHg) period followed by 2 minute period of a target $P_{ET}CO_2$ level, followed by 1 minute of baseline with this cycle repeated 5 times to include $P_{ET}CO_2$ levels of 49, 43, 37, 40 or 46 mmHg, presented in the pseudo-randomised order. $P_{ET}O_2$ was targeted at 100 mmHg throughout the sequence. Following the CO_2 challenge, $P_{ET}CO_2$ was set to baseline for 1 min before returning to spontaneous ventilation on air.

Image Acquisition

MR scanning was performed on a Philips Achieva 3.0T system, with a whole body volume transmit and 8-ch SENSE head receive coil, and a Philips Achieva 7.0T system, with head volume transmit and 16-ch SENSE head receive coil. Axial images were

acquired using a double-echo, single shot EPI sequence (SENSE factor = 2, TE = 16/81 ms with 30 ms readout per echo at 3T, TE = 20/57 ms with 37 ms readout per echo at 7T); TE values were optimised for R_2* measurement rather than BOLD contrast, 192x192 mm FOV, 2x2x3 mm^3 voxels with 9/10 slices (3T/7T), and no slice gap, in a TR of 1.5 s. Figure 3 shows the typical slice coverage at both 7 and 3 T. For tissue segmentation inversion-recovery (IR)-EPI images were acquired with the same geometry, with grey matter (GM), white matter (WM) and CSF nulled (TI = 600/900/1900 ms at 3T and TI = 600/1100/2200 ms at 7T). For vein segmentation a high-resolution (0.8mm isotropic) T_2*-weighted fast field echo (FFE) FLASH (TR/TE = 50/20 ms, EPI factor = 3, BW = 167 Hz) image which minimizes geometric distortions was also acquired at 7T.

Data Processing

All data pre-processing was performed using FSL (FMRIB, Oxford, UK). EPI data acquired during the hypercapnic challenge was motion corrected (separately at 3 & 7T) by realigning the shorter TE images to the first dynamic using MCFLIRT (Jenkinson et al. 2002), then applying the registrations to both TE images. R_2* was calculated on a voxel-by-voxel basis from the difference in the log of the signal at each echo time, divided by the difference in echo time. The IR-EPI images were then segmented (BET and FAST, FSL) to generate a GM mask and GM, WM and CSF partial-volume estimates. The WM mask only included voxels that were estimated to be at least 99% WM, to avoid significant partial-voluming from GM reactivity. It was not possible to time lock the MR acquisition and $P_{ET}CO_2$ time course, and so the breath-by-breath $P_{ET}CO_2$ trace was linearly interpolated to match the sampling frequency of the MR data, and then manually shifted to temporally align the $P_{ET}CO_2$ timecourse with the R_2* timecourse averaged over all GM voxels (estimated error is one interpolated time point). This allowed the actual level of $P_{ET}CO_2$ and R_2* to be compared on a point-by-point basis

across a range of $P_{ET}CO_2$ levels (rather than simply comparing the signal change at prescribed $P_{ET}CO_2$ levels). Linear regressions were performed to calculate average GM and WM R_2* CVR to $P_{ET}CO_2$, defining R_2^* CVR as the absolute change in R_2* (measured by the gradient of the linear regression) for a 1 mmHg change in $P_{ET}CO_2$. The fit uncertainties were used to assess the error in R_2* CVR.

The SNR in the R_2* data was not adequate to allow R_2* CVR maps to be produced. Instead BOLD CVR maps were generated combining the double echo data; the SNR in the BOLD data was increased by weighted summation of the EPI images acquired at each echo time (Posse et al. 1999), with the weighting based on a T_2* map calculated from the average baseline signal at both echo times. This was done for each time point and on a voxel-by-voxel basis and the resulting time course was then normalized to the baseline and baseline corrected ((weighted sum signal/average baseline weighted sum signal) – 1), where the baseline was defined as the 40 mmHg $P_{ET}CO_2$ step. For each voxel, the normalized, baseline corrected, summed BOLD signal was plotted against the $P_{ET}CO_2$ signal on a time point by time point basis, after temporal alignment. The gradient of the linear fit to this plot was used to map BOLD CVR on a voxel-by-voxel basis. The fit uncertainties were used to assess the errors in BOLD CVR.

In order to consider the R_2* CVR of tissue alone, excluding large vessels, the FLASH T_2*-weighted image acquired at 7T was used to identify veins, since at 7T veins have a shorter T_2* and so lower signal intensity than the surrounding tissue. Initially regions outside of the brain were removed from the images using the brain extraction tool (BET) in FSL (Smith 2002). The image was then inverted, so that voxels dominated by veins had a high intensity, a third-order polynomial filter was then applied to remove large-scale inhomogeneities and nearest-neighbour smoothing performed. The smoothed image was then subtracted from the unsmoothed image to locate voxels with a significant

venous fraction. Intensity thresholding was performed to produce a binary mask of voxels dominated by veins and cluster analysis performed to remove any isolated voxels. The FLASH image was resized to 2x2x3 mm^3 and co-registered to both the 7T and the 3T EPI datasets and these transformations were then applied to the resized binary mask. This mask was applied to the R_2* time-series to remove these voxels before averaging, thus allowing a comparison of GM and WM R_2* CVR with and without the inclusion of large vessels.

Results

Similar changes in $P_{ET}CO_2$ level were achieved across all subjects. Figure 2 shows a representative subject. Across all subjects the step sizes were consistently a third less than targeted. Despite this, clearly resolvable $P_{ET}CO_2$ transitions were achieved (Fig. 2b) whose level was well maintained over the 2 minute period. The $P_{ET}O_2$ levels reached a steady state within the initial 3 minute baseline period (Fig. 2c) and then had a maximum range of 5 mmHg (across all subjects and all $P_{ET}CO_2$ challenges).

The R_2* time-courses closely followed the $P_{ET}CO_2$ time-course at both field strengths (Fig. 2a). The BOLD CVR maps show good GM contrast at both field strengths (Figure 3) and clear distinction between grey matter and white matter. Increased reactivity is observed in the 7T compared to 3T CVR maps. Table 1 shows individual GM R_2* reactivities both including and excluding voxels dominated by veins. Figure 4(a,b) plots the GM averaged R_2* reactivity at 7 and 3T including data for each of the five subjects. Average GM R_2* reactivities agreed well between subjects (Figure 4). Including voxels dominated by veins, GM R_2* CVR was 2.0±0.4 times higher at 7T than at 3T (averaged over all subjects): GM R_2* CVR was 0.074±0.007 $s^{-1}mmHg^{-1}$ at 3T and 0.145±0.020 $s^{-1}mmHg^{-1}$ at 7T. Excluding voxels dominated by veins GM R_2* reactivity was 2.1±0.5 times higher at 7T than at 3T (averaged over all subjects): GM R_2* CVR was 0.066±0.004

s^{-1} $mmHg^{-1}$ at 3T and 0.141±0.008 $s^{-1}mmHg^{-1}$ at 7T. There was a significant increase in the GM R_2* CVR 7T/3T ratio between the case when vessels were included and when they were excluded (P =0.06, Wilcoxon paired). Contrast-to-noise ratio (CNR) was calculated for GM R_2* CVR as 0.88 $mmHg^{-1}$ at 7T and 0.98 $mmHg^{-1}$ at 3T. This was calculated by dividing the GM R_2* CVR by the variance (GM R_2* standard deviation) of the 40 mmHg $P_{ET}CO_2$ step, averaged over all subjects.

The paradigm provided sufficient sensitivity to detect an average WM R_2* CVR (Table 2) of 0.021±0.003 $s^{-1}mmHg^{-1}$ at 3T and 0.040±0.007 $s^{-1}mmHg^{-1}$ at 7T with veins removed. Figure 4(c,d) plots the WM averaged R_2* reactivity at 7 and 3T for each of the five subjects.

Discussion

This study has combined a versatile and accurate method for controlling and measuring $P_{ET}CO_2$ and $P_{ET}O_2$ with a quantitative R_2* measurement to provide a new time point-by-time point approach to monitoring CVR using MRI. Small, readily tolerable steps in $P_{ET}CO_2$ over a naturally occurring range of $P_{ET}CO_2$ (37 – 49 mmHg) were used. The rapid sampling of the $P_{ET}CO_2$ and MR data allowed point-by-point temporal analysis which improved sensitivity in CVR, allowing measurement of GM reactivity and detection of significant WM reactivity, at both 3 and 7T.

The technique to control blood gases used in this study allowed independent control of $P_{ET}CO_2$ and $P_{ET}O_2$, to provide transitions to and between stable $P_{ET}CO_2$ levels, whilst maintaining $P_{ET}O_2$ at a constant level (Slessarev et al. 2007). $P_{ET}CO_2$ transitions were achieved within one or two breaths. It is essential that a constant level of $P_{ET}O_2$ is maintained, as the BOLD signal is modulated by the O_2 content (hyperoxia) of the blood which could otherwise confound the relationship between CBF changes and BOLD signal (Prisman et al. 2008). Increasing P_aO_2 above resting levels, in which arterial haemoglobin

is near fully oxygenated, dissolves more O_2 in blood plasma. This pool of O_2 then spares the O_2 that would be extracted from oxygenated-haemoglobin, and thus reduces the venous [dHb]. To date, few approaches that change $P_{ET}CO_2$ to probe the relationship between hypercapnia and BOLD signal have controlled $P_{ET}O_2$. Simple breath holding, which has the advantage of requiring no additional equipment (Kastrup et al. 2001; Scouten and Schwarzbauer 2008), does not generate repeatable stimulus levels (due to inter-subject and inter-session variability in resting metabolism) (Bulte et al. 2009), does not allow lung gas to be monitored during the breath-hold (as no gas is exhaled), and produces a coupled reduction in P_aO_2 (Sasse et al. 1996). Alternatively, $P_{ET}CO_2$ is often modulated by providing two different inspired gas mixtures, typically containing oxygen, nitrogen and either 0% CO_2 (baseline) or 5% CO_2 (hypercapnic challenge) (Davis et al. 1998; Cohen et al. 2004; Wise et al. 2007). However the level of $P_{ET}CO_2$ that is achieved using such a method depends on the particular ventilatory response of the volunteer. Since inhaling CO_2 causes hyperventilation, $P_{ET}O_2$ will rise even if the inspired PO_2 is constant. $P_{ET}CO_2$ and $P_{ET}O_2$ can be controlled independently by a method termed dynamic end-tidal forcing (Wise et al. 2007). This method uses a computer controlled feedback mechanism to correct the supplied gas concentrations based on breath-by-breath sampling of $P_{ET}CO_2$ and $P_{ET}O_2$. However, feedback mechanisms are hampered by the delay and dampening of the exhaled gas changes over the time they take to reach the gas sensors, which have to be positioned far from the subject in high-field experiments. Thus with dynamic end-tidal forcing, $P_{ET}CO_2$ may not provide a good estimate of P_aCO_2 (St Croix et al. 1995).

Previously, T_2* (not R_2*) CVR has been measured (Posse et al. 2001), with a non-linear relationship observed over large (10 mmHg) $P_{ET}CO_2$ steps. $P_{ET}O_2$ was not controlled and the high gas flow rates used to achieve high (70 mmHg) and low (20

mmHg) $P_{ET}CO_2$ target levels would have induced hyperventilation, leading to increased $P_{ET}O_2$ (not monitored), arterial oxygenation and a further increase in T_2*, which may have accounted for some of the non-linearity. However, a rough conversion of their results from T_2* to R_2*(=1/T_2*) shows an approximately linear relationship between R_2* and $P_{ET}CO_2$ from 40-60 mmHg.

This study used high spatial resolution compared to previous CVR studies, which will have reduced partial volume effects between GM and WM, and allowed us to exclude venous vessels. In this study we found an increase in R_2* CVR with field strength, which is consistent with previous cross-field BOLD CVR studies (Cohen et al. 2004). Removing voxels with large venous components reduced the R_2* CVR at both field strengths, consistent with the intravascular/perivascular signal dominating the BOLD signal change. Furthermore this reduction in reactivity was larger at 3T than 7T. This is expected since the R_2* of blood is much greater at 7T, so the direct signal contribution from blood is reduced.

The results also suggest that the power law relating the change in R_2* to frequency shift (due to change in relative intravascular susceptibility or field strength) is close to linear (7/3=2.3) between 3 and 7 T, and by excluding voxels dominated by veins the 7T:3T R_2* reactivity ratio was increased. Yablonskiy (Yablonskiy and Haacke 1994) predicted a linear relationship for extravascular dephasing if vessels were assumed to be randomly orientated. A linear relationship between R_2* and frequency offset is expected in the static dephasing regime, whereas supralinear relationships are associated with intermediate and fast dephasing regimes. The effect of diffusion on transverse relaxation around a vein will depend on vessel size and frequency offset due to the vein as well as echo time. For the echo times used here, as the frequency offset increases, the vessel size at which the static dephasing limit dominates decreases (Kennan et al. 1994). Monte Carlo

simulations predict supralinear behaviour at 1.5T (Ogawa et al. 1993; Davis et al. 1998), with 3T being the boundary between linear and supralinear behaviour (Boxerman et al. 1995). It should be noted that the BOLD calibration method (Davis et al. 1998) was first developed at 1.5T and so the power law relationship proposed in that work between intravascular oxygenation and R_2* (1.5) may not be appropriate at higher fields. For WM the power law does seem to be <1. WM has a different vascular structure with much smaller blood volume than GM, and also restricted extravascular water diffusion (due to myelination of the axons), and this might alter the relationship between intravascular susceptibility, the microscopic field distribution in the tissue and the resulting R_2*. However this requires further investigation since WM reactivity data must be interpreted with caution due to the reduced SNR of this data.

The relationship between R_2* and $P_{ET}CO_2$ depends on the relationship between CBF and $P_{ET}CO_2$, CBV and CBF (power law described by Grubb's constant (Grubb et al. 1974)), CBF and venous blood oxygenation, and the resulting relationship between CBV and venous blood oxygenation and R_2*. As discussed above, Monte Carlo simulations and the cross field data presented here and elsewhere (van der Zwaag et al. 2009), suggest the relationship between venous blood oxygenation and R_2* is linear at 3 and 7T. Furthermore it has been shown (Reivich 1964) in anesthetised rhesus monkeys that the relationship between P_aCO_2 and CBF is sigmoidal over the P_aCO_2 range of 5-418 mmHg, centred on the natural resting value of P_aCO_2 of 40 mmHg, but that over the normal range of P_aCO_2 values the relationship between P_aCO_2 and CBF is linear (in that study changes in P_aO_2 were also found to have no effect on CBF). Therefore the simplest interpretation of the linear relationship observed here would be that the relationship between CBF and CBV is linear (ie Grubbs constant =1), although this assumes that the relationship between CBF and oxygenation is approximately linear. However this argument is made

for a global challenge and may not be appropriate when considering the effects of local challenges (e.g. response to neuronal activation) where the haemodynamic effects may be somewhat different.

In this study, the gas sampling data could not be electronically time locked to the scanner acquisition due to hardware limitations, and so the respiratory sequence was manually synchronized with the imaging sequence (~ ± 1.5s). There was also a delay between gas delivery and sampling of about 5 seconds caused by the transit time between the mask and the gas sensors residing outside the 3mT magnetic field line. The data signals therefore had to be aligned manually during processing, and so it was not possible to estimate the delay between the $P_{ET}CO_2$ change and associated CVR. This could potentially add noise to the R_2* CVR curves but this effect will not be significant since the $P_{ET}CO_2$ data were resampled from ~6s sampling interval to 1.5s sampling interval. It is interesting to note that there was a close correlation between $P_{ET}CO_2$ stimulus and the associated BOLD response on both the up and down transitions, with no sign of a post stimulus undershoot, suggesting that the post stimulus undershoot often observed in the BOLD signal evoked by neuronal activation is not vascular in origin (Mandeville et al. 1999), although further experiments are required to confirm this conclusion.

The echo times used in this study were chosen to optimize the estimate of R_2*, although hardware limitations meant that the optimal (short) echo times required at 7T could not be reached. Therefore although better contrast was achieved at 7T, similar contrast-to-noise was observed at both field strengths in GM due to the non-optimal TE and increased physiological noise at 7T, shown by increased R_2* variance at 7T over 3T ($p<0.003$). This agrees with the findings of Triantafyllou et al. (Triantafyllou et al. 2005). Respiratory noise was particularly pronounced because of pacing of the respiratory cycle and because the subjects increased their depth of breathing during the respiratory

challenge. This can be seen in Figure 2a, where there is a ~6s oscillation throughout the BOLD timecourses. Physiological noise correction methods, such as RETROICOR (Glover et al. 2000) could be used in future work to reduce the respiratory noise, although this would require an additional measurement of chest movement. However the RETROICOR algorithm employs a high-pass filter for linear de-trending, which will also remove some of the reactivity for the paradigm used here, especially as the stimulus is time-locked to the respiratory cycle. An alternative to retrospective correction is to actively perform dynamic shimming (van Gelderen et al. 2007) to correct for the gradient changes through the respiratory cycle. A sinusoidal CO_2 stimulus (Blockley et al. 2009) might be less affected by respiratory noise if the stimulus frequency were made significantly different from the respiratory noise frequency.

During a long fMRI experiment, variations in P_aCO_2 that are likely to occur as a subject relaxes, will lead to a baseline drift in the BOLD signal. This study has shown that R_2* reactivity to P_aCO_2 is linear over the typical range of these changes, and so to the first approximation (for a small change in R_2*) the effect can be removed simply by linear de-trending of the BOLD signal time course. However if the functional stimulus also caused changes in P_aCO_2, through changes during the respiratory cycle (e.g. where the stress of performing a task increases respiration), then the resulting BOLD signal change would be on the same timescale as the functional BOLD response, producing a systematic error in the fMRI response.

An alternative MR-based method for monitoring CVR with MRI could be to use arterial spin labelling (ASL) to measure CBF. Mandell (Mandell et al. 2008) found a close correlation between BOLD and ASL measurements of CVR. Although ASL based methods are a more direct measurement of CVR, they have an intrinsically lower signal-to-noise ratio and they generally provide a lower temporal resolution than BOLD.

However combined measurements of CBF and R_2* changes in response to CVR to $P_{ET}CO_2$ could provide useful information with which to test models of aspects of cerebral haemodynamic changes in response to neuronal activation (Buxton et al. 1998; Blockley et al. 2009).

Future work will use this paradigm in clinical studies of cerebrovascular disease (van der Zande et al. 2005; Mandell et al. 2008) and will use the respiratory challenge to investigate the steady state relationship between CBF, blood volume and blood oxygenation.

Acknowledgements

This work was funded by the UK Medical Research Council and Engineering and Physical Sciences Research Council.

Tables

GM average including venous voxels	R_2* reactivity ($s^{-1}mmHg^{-1}$)		
	7T	3T	7T/3T
Subject 1	-0.173±0.005	-0.067±0.004	2.6
Subject 2	-0.146±0.009	-0.086±0.005	1.7
Subject 3	-0.163±0.008	-0.072±0.004	2.3
Subject 4	-0.133±0.010	-0.075±0.002	1.8
Subject 5	-0.109±0.006	-0.073±0.005	1.5
Mean (across subjects) ± Standard deviation	-0.145±0.025	-0.074±0.007	2.0±0.4

GM average with venous voxels excluded	R_2* reactivity ($s^{-1}mmHg^{-1}$)		
	7T	3T	7T/3T
Subject 1	-0.168±0.005	-0.058±0.004	2.9
Subject 2	-0.134±0.009	-0.081±0.005	1.7
Subject 3	-0.163±0.008	-0.070±0.004	2.4
Subject 4	-0.128±0.009	-0.065±0.002	2.0
Subject 5	-0.109±0.006	-0.060±0.005	1.8
Mean (across subjects) ± Standard deviation	-0.141±0.025	-0.066±0.009	2.1±0.5

Table 1: GM R_2* reactivity for all subjects, calculated using a linear regression.

WM average with venous voxels excluded	R_2* reactivity ($s^{-1}mmHg^{-1}$)		
	7T	3T	7T/3T
Subject 1	-0.035±0.006	-0.001±0.002	*31.7
Subject 2	-0.031±0.011	-0.020±0.002	1.6
Subject 3	-0.061±0.009	-0.028±0.004	2.2
Subject 4	-0.050±0.005	-0.036±0.003	1.4
Subject 5	-0.022±0.004	-0.020±0.002	1.1
Mean (across subjects) ± Standard deviation	-0.040±0.015	-0.021±0.013	*1.6±0.5

Table 2: WM R_2* reactivity for all subjects, calculated using a linear regression.*The 7T/3T ratio for Subject 1 is treated as an outlier and has been ignored in the cross-subject mean calculation.

Figures

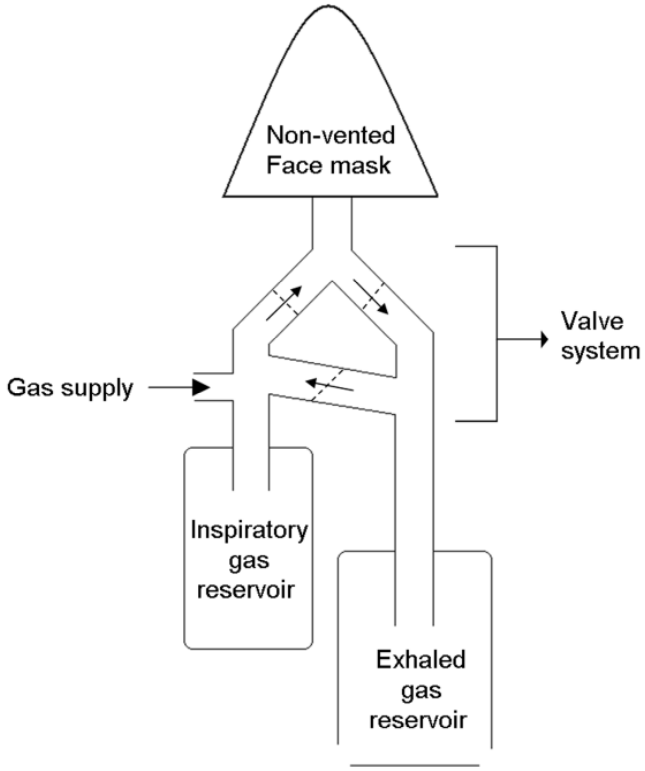

Figure 1: Sequential Gas Delivery (SGD) circuit, based on Slessarev (2007). Upon inspiration, gas flows from the inspiratory gas reservoir to the mask. If the inspiratory gas reservoir is collapsed, the valves switch so that gas from the exhaled gas reservoir flows into the mask. Upon expiration, the valves prevent exhaled gas from entering the inspiratory gas reservoir. The exhaled gas reservoir features two slits in the bottom corners which act as vents.

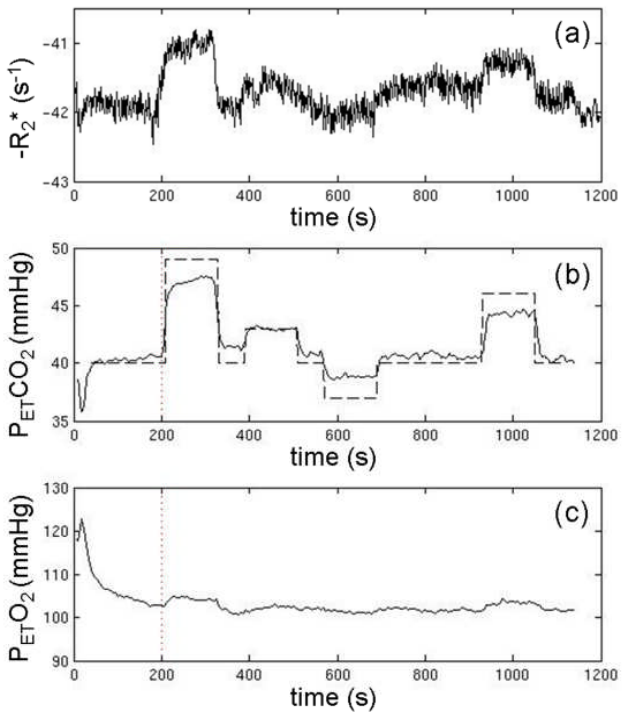

Figure 2: Corresponding time-courses for (a) GM average $-R_2^*$ (veins excluded), measured (b) $P_{ET}CO_2$ and (c) $P_{ET}O_2$. $-R_2^*$ is plotted to show the tight linear correlation between $P_{ET}CO_2$ and $-R_2^*$. The dotted vertical line indicates the end of the initial baseline period. The dashed trace shows targeted $P_{ET}CO_2$ levels. (Subject #5 at 7T)

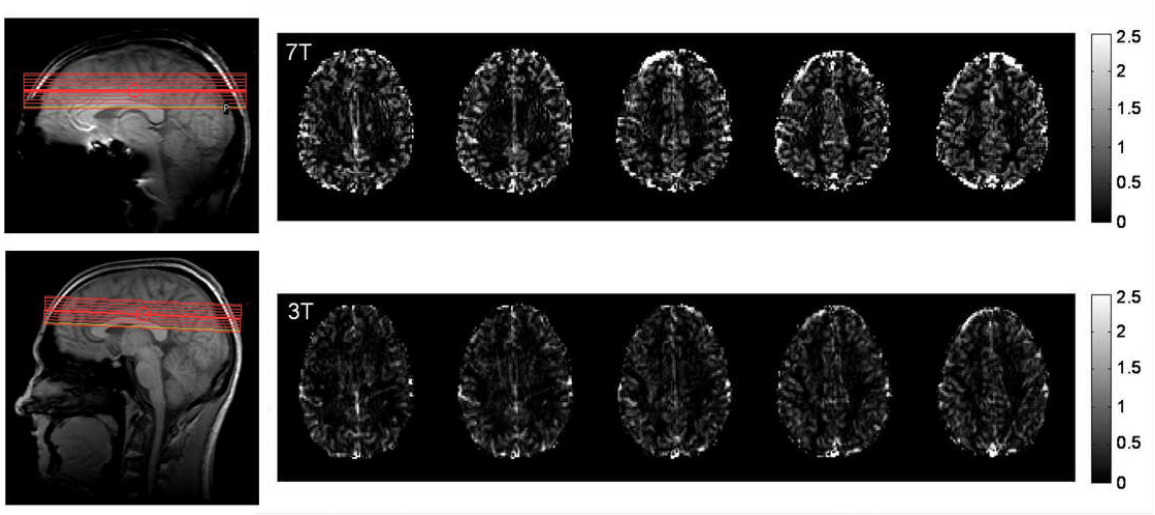

Figure 3: Localiser showing typical slice coverage and corresponding CVR maps of subject #5 at 7T and 3T. The scale ranges from 0 to 2.5%/mmHg signal change and the middle 5 slices are shown.

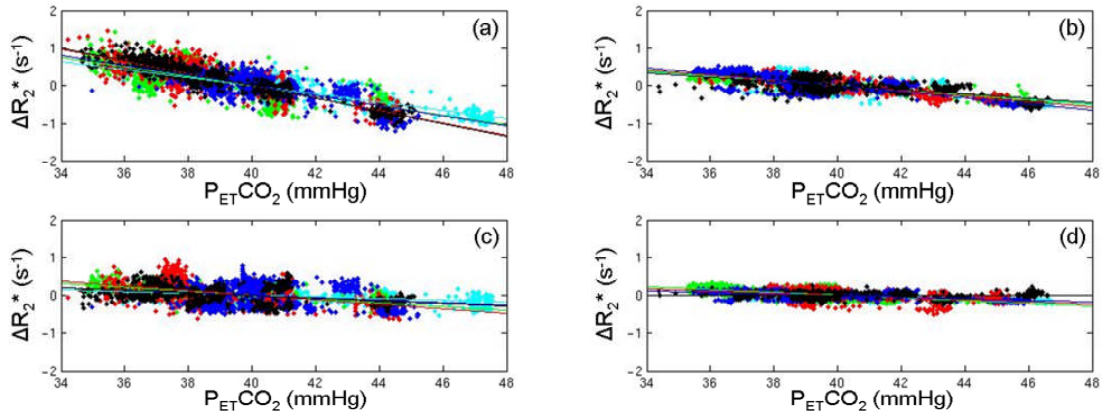

Figure 4: GM averaged R_2* reactivity at (a) 7T and (b) 3T and WM averaged R_2* reactivity at (c) 7T and (d) 3T for all subjects (veins excluded). Averaged R_2* reactivity is shown by the scatter plots and linear fits are shown as lines. Each subject is plotted in a different colour.

References

Banzett, R. B., R. T. Garcia and S. H. Moosavi, 2000. Simple contrivance "clamps" end-tidal Pco(2) and Po-2 despite rapid changes in ventilation. J. Appl. Physiol. 88(5), 1597-1600.

Blockley, N. P., I. D. Driver, S. T. Francis, J. A. Fisher and P. A. Gowland 2009. Sinusoidally modulated CO2 stimulus provides new temporal information on cerebrovascular reactivity. Proc. Intl. Soc. Mag. Reson. Med., Honolulu, Hawaii, USA.17, 1632.

Blockley, N. P., S. T. Francis and P. A. Gowland, 2009. Perturbation of the BOLD response by a contrast agent and interpretation through a modified balloon model. Neuroimage 48(1), 84-93.

Boxerman, J. L., L. M. Hamberg, B. R. Rosen and R. M. Weisskoff, 1995. MR contrast due to intravascular magnetic-susceptibility perturbations. Magn. Reson. Med. 34(4), 555-566.

Bulte, D. P., K. Drescher and P. Jezzard, 2009. Comparison of Hypercapnia-Based Calibration Techniques for Measurement of Cerebral Oxygen Metabolism With MRI. Magn. Reson. Med. 61(2), 391-398.

Buxton, R. B., E. C. Wong and L. R. Frank, 1998. Dynamics of blood flow and oxygenation changes during brain activation: The balloon model. Magn. Reson. Med. 39(6), 855-864.

Chen, J. J. and G. B. Pike 2009. Does Global Cerebral Oxygen Metabolism Change During Hypercapnia and Hypocapnia in Awake Humans? Proc. Intl. Soc. Mag. Reson. Med., Honolulu, Hawaii, USA.17, 214.

Cohen, E. R., E. Rostrup, K. Sidaros, T. E. Lund, O. B. Paulson, K. Ugurbil and S. G. Kim, 2004. Hypercapnic normalization of BOLD fMRI: comparison across field strengths and pulse sequences. Neuroimage 23(2), 613-624.

Davis, T. L., K. K. Kwong, R. M. Weisskoff and B. R. Rosen, 1998. Calibrated functional MRI: Mapping the dynamics of oxidative metabolism. Proc. Natl. Acad. Sci. U. S. A. 95(4), 1834-1839.

Glover, G. H., T. Q. Li and D. Ress, 2000. Image-based method for retrospective correction of physiological motion effects in fMRI: RETROICOR. Magn. Reson. Med. 44(1), 162-167.

Grubb, R. L., M. E. Raichle, J. O. Eichling and Terpogos.Mm, 1974. Effects of changes in PaCO2 on cerebral blood volume, blood flow, and vascular mean transit time. Stroke 5(5), 630-639.

Hoge, R. D., J. Atkinson, B. Gill, G. R. Crelier, S. Marrett and G. B. Pike, 1999. Investigation of BOLD signal dependence on cerebral blood flow and oxygen consumption: The deoxyhemoglobin dilution model. Magn. Reson. Med. 42(5), 849-863.

Ito, S., A. Mardimae, J. Han, J. Duffin, G. Wells, L. Fedorko, L. Minkovich, R. Katznelson, M. Meineri, T. Arenovich, C. Kessler and J. A. Fisher, 2008. Non-invasive prospective targeting of arterial P-CO2 in subjects at rest. J. Physiol.-London 586(15), 3675-3682.

Jenkinson, M., P. Bannister, M. Brady and S. Smith, 2002. Improved optimization for the robust and accurate linear registration and motion correction of brain images. Neuroimage 17(2), 825-841.

Kastrup, A., G. Kruger, T. Neumann-Haefelin and M. E. Moseley, 2001. Assessment of cerebrovascular reactivity with functional magnetic resonance imaging: comparison of CO2 and breath holding. Magn. Reson. Imaging 19(1), 13-20.

Kennan, R. P., J. H. Zhong and J. C. Gore, 1994. Intravascular susceptibility contrast mechanisms in tissues. Magn. Reson. Med. 31(1), 9-21.

Mandell, D. M., J. S. Han, J. Poublanc, A. P. Crawley, J. A. Stainsby, J. A. Fisher and D. J. Mikulis, 2008. Mapping cerebrovascular reactivity using blood oxygen level-dependent MRI in patients with arterial steno-occlusive disease - Comparison with arterial spin labeling MRI. Stroke 39(7), 2021-2028.

Mandeville, J. B., J. J. A. Marota, C. Ayata, G. Zaharchuk, M. A. Moskowitz, B. R. Rosen and R. M. Weisskoff, 1999. Evidence of a cerebrovascular postarteriole windkessel with delayed compliance. J. Cereb. Blood Flow Metab. 19(6), 679-689.

Noth, U., G. E. Meadows, F. Kotajima, R. Deichmann, D. R. Corfield and R. Turner, 2006. Cerebral vascular response to hypercapnia: Determination with perfusion MRI at 1.5 and 3.0 tesla using a pulsed arterial spin labeling technique. J. Magn. Reson. Imaging 24(6), 1229-1235.

Ogawa, S., R. S. Menon, D. W. Tank, S. G. Kim, H. Merkle, J. M. Ellermann and K. Ugurbil, 1993. Functional brain mapping by blood oxygenation level-dependent contrast magnetic-resonance-imaging- A comparison of signal characteristics with a biophysical model. Biophysical Journal 64(3), 803-812.

Pollock, J. M., A. R. Deibler, C. T. Whitlow, H. Tan, R. A. Kraft, J. H. Burclette and J. A. Maldjian, 2009. Hypercapnia-Induced Cerebral Hyperperfusion: An Underrecognized Clinical Entity. Am. J. Neuroradiol. 30(2), 378-385.

Posse, S., L. J. Kemna, B. Elghahwagi, S. Wiese and V. G. Kiselev, 2001. Effect of graded hypo- and hypercapnia on fMRI contrast in visual cortex: Quantification of T-2* changes by multiecho EPI. Magn. Reson. Med. 46(2), 264-271.

Posse, S., S. Wiese, D. Gembris, K. Mathiak, C. Kessler, M. L. Grosse-Ruyken, B. Elghahwagi, T. Richards, S. R. Dager and V. G. Kiselev, 1999. Enhancement of BOLD-contrast sensitivity by single-shot multi-echo functional MR imaging. Magn. Reson. Med. 42(1), 87-97.

Prisman, E., M. Slessarev, J. Han, J. Poublanc, A. Mardimae, A. Crawley, J. Fisher and D. Mikulis, 2008. Comparison of the effects of independently-controlled end-tidal PCO2 and PO2 on blood oxygen level-dependent (BOLD) MRI. J. Magn. Reson. Imaging 27(1), 185-191.

Reivich, M., 1964. Arterial PCO2 and cerebral hemodynamics. Am. J. Physiol. 206(1), 25-&.

Sasse, S. A., R. B. Berry, T. K. Nguyen, R. W. Light and C. K. Mahutte, 1996. Arterial blood gas changes during breath-holding from functional residual capacity. Chest 110(4), 958-964.

Scouten, A. and C. Schwarzbauer, 2008. Paced respiration with end-expiration technique offers superior BOLD signal repeatability for breath-hold studies. Neuroimage 43(2), 250-257.

Slessarev, M., J. Han, A. Mardimae, E. Prisman, D. Preiss, G. Volgyesi, C. Ansel, J. Duffin and J. A. Fisher, 2007. Prospective targeting and control of end-tidal CO2 and O-2 concentrations. J. Physiol.-London 581(3), 1207-1219.

Smith, S. M., 2002. Fast robust automated brain extraction. Hum Brain Mapp 17(3), 143-55.

St Croix, C. M., D. A. Cunningham, J. M. Kowalchuk, A. K. McConnell, A. S. Kirby, B. W. Scheuermann, R. J. Petrella and D. H. Paterson, 1995. Estimation of arterial PCO2 in the elderly. J. Appl. Physiol. 79(6), 2086-2093.

Stefanovic, B., J. M. Warnking, K. M. Rylander and G. B. Pike, 2006. The effect of global cerebral vasodilation on focal activation hemodynamics. Neuroimage 30(3), 726-734.

Triantafyllou, C., R. D. Hoge, G. Krueger, C. J. Wiggins, A. Potthast, G. C. Wiggins and L. L. Wald, 2005. Comparison of physiological noise at 1.5 T, 3 T and 7 T and optimization of fMRI acquisition parameters. Neuroimage 26(1), 243-250.

van der Zande, F. H. R., P. A. M. Hofman and W. H. Backes, 2005. Mapping hypercapnia-induced cerebrovascular reactivity using BOLD MRI. Neuroradiology 47(2), 114-120.

van der Zwaag, W., S. Francis, K. Head, A. Peters, P. Gowland, P. Morris and R. Bowtell, 2009. fMRI at 1.5, 3 and 7 T: Characterising BOLD signal changes. Neuroimage 47(4), 1425-1434.

van Gelderen, P., J. A. de Zwart, P. Starewicz, R. S. Hinks and J. H. Duyn, 2007. Real-time shimming to compensate for respiration-induced B-0 fluctuations. Magn. Reson. Med. 57(2), 362-368.

Vesely, A., H. Sasano, G. Volgyesi, R. Somogyi, J. Tesler, L. Fedorko, J. Grynspan, A. Crawley, J. A. Fisher and D. Mikulis, 2001. MRI mapping of cerebrovascular reactivity using square wave changes in end-tidal PCO2. Magn. Reson. Med. 45(6), 1011-1013.

Wise, R. G., K. T. S. Pattinson, D. P. Bulte, P. A. Chiarelli, S. D. Mayhew, G. M. Balanos, D. F. O'Connor, T. R. Pragnell, P. A. Robbins, I. Tracey and P. Jezzard, 2007. Dynamic forcing of end-tidal carbon dioxide and oxygen applied to

functional magnetic resonance imaging. J. Cereb. Blood Flow Metab. 27(8), 1521-1532.

Yablonskiy, D. A. and E. M. Haacke, 1994. Theory of NMR signal behaviour in magnetically inhomogeneous tissues - The Static Dephasing Regime. Magn. Reson. Med. 32(6), 749-763.

Yacoub, E., A. Shmuel, J. Pfeuffer, P. F. Van De Moortele, G. Adriany, P. Andersen, J. T. Vaughan, H. Merkle, K. Ugurbil and X. Hu, 2001. Imaging brain function in humans at 7 Tesla. Magn Reson Med 45(4), 588-94.